Arch. Mech., 46, 1–2, pp. 13–36, Warszawa 1994

Analysis of dynamic shear bands in porous thermally softening viscoplastic materials

R. C. BATRA and X. S. JIN (BLACKSBURG)

WE STUDY THE INITIATION and growth of shear bands in a porous thermally softening viscoplastic block of square cross-section and deformed in plane strain tension. The impact load is modelled by prescribing a time-dependent axial velocity on the top and bottom surfaces which are taken to be free of the tangential tractions.The material defect is modelled by assuming that the material in a small region surrounding the centroid of the cross-section is weaker than the rest of the material. The finite element mesh consisting of constant strain triangular elements is refined adaptively so that the integral of the effective plastic strain-rate over an element is nearly the same for all elements in the mesh. The effects of the presumed variation in the initial porosity and the impact speed on the nominal strain at which a shear band initiates have been examined. For a typical steel alloy, we have also ascertained the effect, on the initiation of the shear band, of the softening caused by the increase in the porosity and/or the increase in the temperature.

1. Introduction

MICROSCOPIC OBSERVATIONS [1–10] of the failure process in several metallic alloys (e.g., AISI 1018 cold-rolled steel, AISI 4340 vacuum arc remelted steel, HY-100 steel, titanium and titanium alloys) have revealed that fracture occurs by a process of nucleation and coalescence of voids and microcracks. Under dynamic loads, the fracture of the specimen is usually preceded by the formation of a shear band [1-6], which is a narrow region, a few micrometers (μm) wide, of intense plastic deformation that forms during high strain-rate processes such as shock loading, ballistic penetration, metal forming, machining, grinding, high speed fabrication, and explosive fragmentation. ZENER and HOLLOMON [11] observed 32 μm wide shear bands during the punching of a hole in a low carbon steel plate, and postulated that the heat generated due to plastic working made the material softer, and the material became unstable when the thermal softening equalled or exceeded the hardening of the material due to strain and strain-rate effects. Since then, there have been numerous analytical, numerical, and experimental studies aimed at analyzing the initiation and growth of shear bands; the reader is referred to SHAWKI and CLIFTON [12] and BATRA and ZHU [13] for a list of references. Our objective here is to delineate the effect of additional softening caused by the nucleation of voids on the formation of shear bands in a prismatic body made of a thermally softening viscoplastic material and deformed in plane strain tension.

A general theory of elastic materials with voids has been developed by NUNZIATO and COWIN [14] and phenomenological constitutive relations for porous ductile solids have been proposed by KUHN and DOWNEY [15], GREEN [16],

GURSON [17], and SHIMA and OYANE [18]. Gurson's model has been modified by TVERGAARD [19, 20], TVERGAARD and NEEDLEMAN [21], and PAN *et al.* [22] to include work hardening, strain-rate hardening and a generalization of the flow potential. The phenomenon of shear strain localization in porous materials has been studied by PAN *et al.* [22], SAJE *et al.* [23], KOBAYASHI and DODD [24], and ZAVALIANGOS and ANAND [25]. Here we study a dynamic two-dimensional problem and account for the effect of inertia forces and the dependence of the thermophysical properties of the material upon the porosity. Also we use adaptively refined finite element meshes to analyze the problem. The voids are assumed to grow due to plastic dilatation, and a plastic strain controlled nucleation criterion is used to account for the nucleation of voids throughout the deformation history.

2. Formulation of the problem

We assume that voids are randomly distributed throughout the body and denote their volume fraction by f. In terms of the referential description, the thermomechanical deformations of the body are governed by the following equations:

balance of mass

$$(\rho J(1-f))^{\cdot} = 0, \tag{2.1}$$

balance of linear momentum

$$\rho_r(1-f_r)\,\dot{\mathbf{v}} = \operatorname{Div}\mathbf{T}, \tag{2.2}$$

balance of moment of momentum

$$\mathbf{T}\mathbf{F}^T = \mathbf{F}\mathbf{T}^T, \tag{2.3}$$

balance of internal energy

$$\rho_r(1-f_r)\,\dot{e} = -\operatorname{Div}\mathbf{Q} + \operatorname{tr}\left(\mathbf{T}\,\dot{\mathbf{F}}^T\right), \tag{2.4}$$

where

$$\mathbf{F} = \operatorname{Grad}\mathbf{x} \tag{2.5}$$

is the deformation gradient, $\mathbf{x}$ is the present position of a material particle that occupied place $\mathbf{X}$ in the reference configuration, $J = \det\mathbf{F}$, ρ is the present mass density of the matrix or void-free material, ρ_r its mass density in the reference configuration, f_r equals the volume fraction of voids in the reference configuration, $\mathbf{v}$ is the velocity of a material particle, $\mathbf{T}$ is the first Piola–Kirchhoff stress tensor, e is the specific internal energy for the matrix, $\mathbf{Q}$ is the heat flux per

unit undeformed area, a superimposed dot indicates a material time derivative, and Grad and Div signify, respectively, the gradient and the divergence operators applied to a field quantity defined as a function of $\mathbf{X}$ and time t. We have neglected the balance of equilibrated forces considered by NUNZIATO and COWIN [14], and have also assumed that the supplies of linear momentum and internal energy equal zero.

We presume that the strain-rate tensor $\mathbf{D}$, defined by

$$2\mathbf{D} = \operatorname{grad}\mathbf{v} + (\operatorname{grad}\mathbf{v})^T, \tag{2.6}$$

with grad denoting the gradient operator applied to a field quantity defined as a function of $\mathbf{x}$ and t, has the additive decomposition into elastic $\mathbf{D}^e$ and plastic $\mathbf{D}^p$ parts, and make the following constitutive assumptions:

$$\dot{\boldsymbol{\sigma}} + \boldsymbol{\sigma}\boldsymbol{\Omega} - \boldsymbol{\Omega}\boldsymbol{\sigma} = \frac{E(1-f)}{(1+\nu)}(\mathbf{D}-\mathbf{D}^p) + \frac{E\nu(1-f)}{(1+\nu)(1-2\nu)}(\operatorname{tr}(\mathbf{D}-\mathbf{D}^p) - \alpha\dot{\theta})\mathbf{1}, \tag{2.7}$$

$$\Phi = \frac{3}{2}\frac{\operatorname{tr}(\mathbf{s}\,\mathbf{s}^T)}{\sigma_m^2} + 2f^*\beta_1\cosh\left(\frac{\beta_2\operatorname{tr}\boldsymbol{\sigma}}{2\sigma_m}\right) - 1 - \beta_1^2 f^{*2} = 0, \tag{2.8}$$

$$\mathbf{s} = \boldsymbol{\sigma} - \frac{1}{3}(\operatorname{tr}\boldsymbol{\sigma})\mathbf{1}, \tag{2.9}$$

$$\mathbf{D}^p = \frac{(1-f)\sigma_m\,\dot{\bar{\varepsilon}}_m^p}{\operatorname{tr}(\boldsymbol{\sigma}\mathbf{N}^T)}\mathbf{N}, \tag{2.10}$$

$$\mathbf{N} = \frac{3}{\sigma_m^2}\left(\boldsymbol{\sigma} - \frac{1}{3}(\operatorname{tr}\boldsymbol{\sigma})\mathbf{1}\right) + \frac{f^*\beta_1\beta_2}{\sigma_m}\left[\sinh\left(\frac{\beta_2\operatorname{tr}\boldsymbol{\sigma}}{2\sigma_m}\right)\right]\mathbf{1}, \tag{2.11}$$

$$f^* = \begin{cases} f & \text{if} \quad f \le f_c, \\ f_c + \left(\dfrac{f_u^* - f_c}{f_f - f_c}\right)(f - f_c) & \text{otherwise,} \end{cases} \tag{2.12}$$

$$\sigma_m = \sigma_0\left(1 + b\,\dot{\bar{\varepsilon}}_m^p\right)^m\left(1 + \frac{\bar{\varepsilon}_m^p}{\varepsilon_y}\right)^n(1 - \nu_s\theta), \tag{2.13}$$

$$\dot{f} = (1-f)\operatorname{tr}\mathbf{D}^p + \frac{f_2\,\dot{\bar{\varepsilon}}_m^p}{s_2\sqrt{2\pi}}\exp\left(-\frac{1}{2}\left(\frac{\bar{\varepsilon}_m^p - e_N}{s_2}\right)^2\right), \tag{2.14}$$

$$\mathbf{q} = -k\left(1 - \frac{3}{2}f\right)\operatorname{grad}\theta, \tag{2.15}$$

$$\dot{e} = c\,\dot{\theta} + \operatorname{tr}(\boldsymbol{\sigma}(\mathbf{D} - \mathbf{D}^p)), \tag{2.16}$$

where

$$\mathbf{T} = J\boldsymbol{\sigma}\left(\mathbf{F}^{-1}\right)^{T}, \tag{2.17}$$

$$\mathbf{Q} = J\mathbf{F}^{-1}\mathbf{q}, \tag{2.18}$$

$$2\boldsymbol{\Omega} = \operatorname{grad}\mathbf{v} - (\operatorname{grad}\mathbf{v})^{T}. \tag{2.19}$$

Equation (2.7) is Hooke's law written in the rate form with the left-hand side equal to the Jaumann derivative of the Cauchy stress tensor $\boldsymbol{\sigma}$, $\boldsymbol{\Omega}$ defined by Eq. (2.19) is the skew-symmetric part of the velocity gradient, E, ν, and α, respectively, are Young's modulus, Poisson's ratio, and the coefficient of thermal expansion for the matrix material, and $\mathbf{1}$ is the unit tensor. We have included the factor $(1 - f)$ on the right-hand side of the constitutive relation (2.7) to account for the porosity of the material; this was also considered by PASSMAN and BATRA [26] and KOBAYASHI and DODD [24]. BUDIANSKY [27] has given the dependence of the material parameters upon f for a macroscopically isotropic composite consisting of a random dispersion of roughly spherical voids in a matrix material. These relations are more involved than the simple reduction of E by the factor $(1 - f)$ we have used in Eq. (2.7). Equations (2.10) and (2.11) follow from the plastic yield function (2.8) proposed by Gurson and subsequently modified by Tvergaard, and the assumptions that $\mathbf{D}^p$ is directed along the outward normal $\mathbf{N}$ to the yield function Φ, and the plastic working $\operatorname{tr}(\boldsymbol{\sigma}\mathbf{D}^p)$ equals $(1-f)\sigma_m\,\dot{\varepsilon}_m^p$ with σ_m and $\dot{\varepsilon}_m^p$ denoting the effective stress and the equivalent plastic strain-rate in the matrix material. The expressions (2.12) for f^* were given by TVERGAARD and NEEDLEMAN [21] so that the computed results matched well the test findings for the cup-cone fracture in a round tensile bar. They suggest the values $f_c \approx 0.15$ and $f_f \approx 0.25$. As $f \to f_f$, $f^* \to f_u^*$, and the material loses all stress-carrying capacity. In Eq. (2.8), β_1 and β_2 are material parameters and $\mathbf{s}$ is the deviatoric Cauchy stress tensor.

Equation (2.13) relating the effective stress σ_m in the matrix to the equivalent plastic strain, equivalent plastic strain-rate, and the temperature is a generalization, due to BATRA [28], to the three-dimensional state of deformation of that proposed by LITOŃSKI [29] for the simple shearing problem. In that equation, σ_0 equals the yield stress of the matrix material in a quasistatic simple compression test, the parameters b and m characterize strain-rate sensitivity of the material, ε_y and n the strain-hardening, and ν_s the thermal softening of the matrix material. The first term on the right-hand side of Eq. (2.14) describes the growth of voids due to plastic dilatation, and the second term describes the plastic strain-controlled nucleation of voids. CHU and NEEDLEMAN [30] suggested this form by assuming that void nucleation follows a normal distribution about some mean critical plastic strain. In Eq. (2.14), s_2 is the standard deviation of the normal distribution, f_2 equals the volume fraction of voids that would be nucleated if deformation continued infinitely, and e_N equals the strain at which the void

nucleation rate reaches a maximum. The experimental studies of LEROY [31] and FISHER [32] on spheroidized carbon steel indicate that, at least in these materials, a void perfusion strain can be identified at which the rate of nucleation is maximal. The void perfusion strain can be taken as e_N. Here we have not considered the stress-controlled nucleation of voids. Equation (2.15) is the Fourier law of heat conduction with $\mathbf{q}$ denoting the heat flux per unit deformed area, and k – the thermal conductivity of the matrix. That the thermal conductivity of the porous materials equals $(1-3/2\ f)$ times that of the matrix material is due to BUDIANSKY [27]. In the constitutive relation (2.16) for the rate of change of internal energy, c is the specific heat for the matrix. Nearly all of the thermophysical material parameters depend upon the temperature. However, such dependences have been neglected for the sake of simplicity.

For a prismatic body of square cross-section, shown in Fig. 1, deformed in plane strain tension, we presume that the deformations are symmetric about the two centroidal axes – and study deformations of the material in the first quadrant. Due to the presumed symmetry of deformations, the normal component

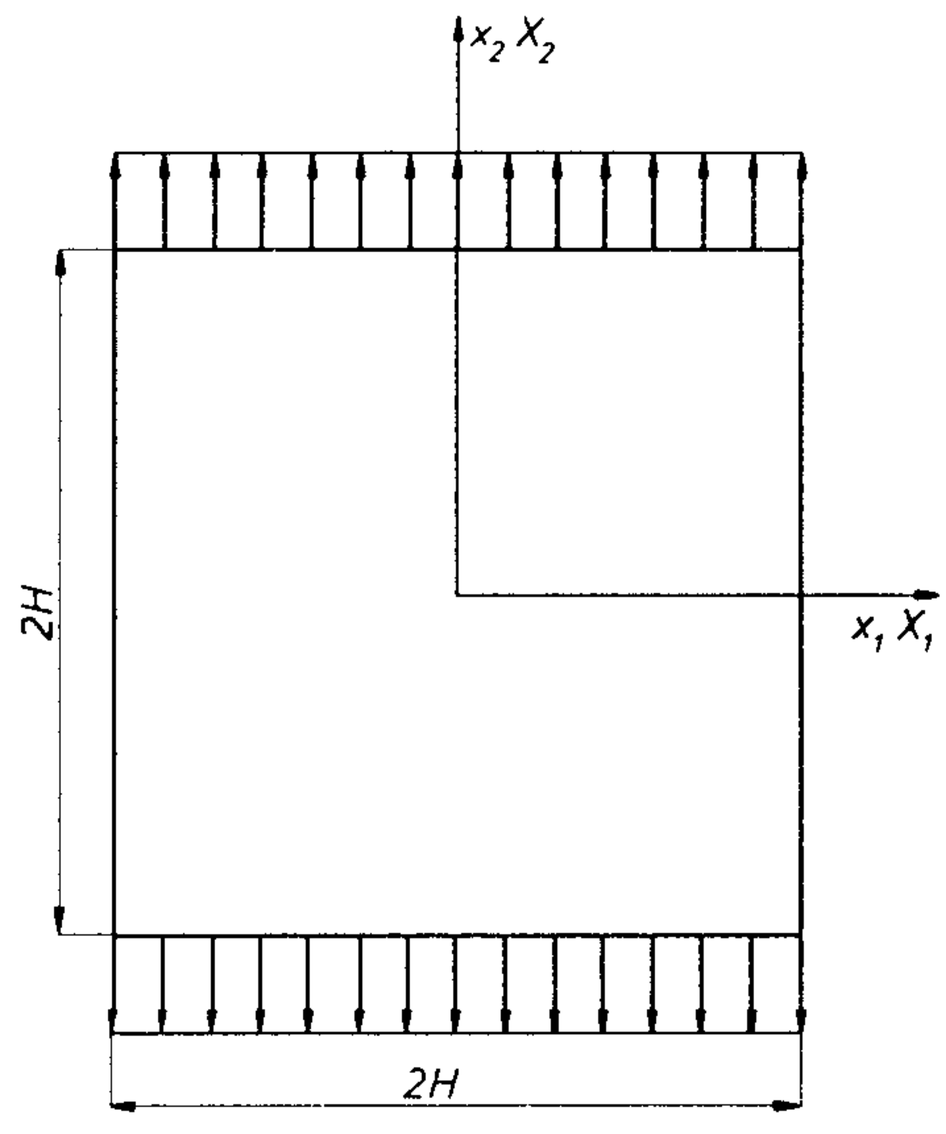

FIG. 1. A schematic sketch of the problem studied.

of velocity and tangential tractions are taken to vanish on the left-hand vertical and bottom horizontal surfaces, the right-hand vertical surface is taken to be traction-free, and on the top horizontal surface, zero tangential tractions and a normal component of velocity, given below, are prescribed;

$$
\begin{aligned}
v_2(X_1, H, t) &= v_0 t/t_r\,, \qquad 0 \le t \le t_r\,, \\
&= v_0, \qquad\qquad t \ge t_r\,.
\end{aligned}
\tag{2.20}
$$

Thus the assigned axial speed on the top surface increases linearly from zero to

the steady value v_0 in time t_r giving an eventual nominal strain-rate of v_0/H. All the bounding surfaces of the block are taken to be thermally insulated.

Initially the block is assumed to be at rest, stress-free and at a uniform temperature θ_0. However, the initial porosity is taken to be non-uniform and given by

$$f(X_1, X_2, 0) = f_0 + \varepsilon(1 - r^2)^9 e^{-5r^2}, \qquad r^2 = (X_1^2 + X_2^2)/H^2. \tag{2.21}$$

The second term on the right-hand side of Eq. $(2.21)_1$ models a material defect or inhomogeneity, the value of ε is a measure of the strength of the defect.

The aforestated coupled and nonlinear partial differential equations (2.1) through (2.19) under the prescribed initial and boundary conditions are too difficult to be analyzed analytically. Therefore, we seek their numerical solution.

3. Computational considerations

In order to solve the problem numerically, we first rewrite Eq. (2.13) as

$$\dot{\varepsilon}_m^p = \max\left[0, \frac{1}{b}\left(\left(\frac{\sigma_m}{\sigma_0\left(\left(1 + \frac{\varepsilon_m^p}{\varepsilon_y}\right)^n (1 - \nu_s\theta)\right)}\right)^{\frac{1}{m}} - 1\right)\right]. \tag{3.1}$$

Thus the equivalent plastic strain-rate is positive only when

$$\sigma_m > \sigma_0\left(1 + \frac{\varepsilon_m^p}{\varepsilon_y}\right)^n (1 - \nu_s\theta), \tag{3.2}$$

otherwise it equals zero implying thereby that all components of plastic strain-rate tensor at the material point under consideration and at that instant vanish identically. The value of σ_m is computed from the yield function (2.8) once $\boldsymbol{\sigma}$ or $\mathbf{s}$ has been found.

By substituting from the constitutive relations into the balance laws, we obtain evolution equations for ρ, $\mathbf{v}$ and θ which, when combined with Eqs. (2.7), (2.14) and (3.2), give a system of equations for the determination of ρ, $\mathbf{v}$, θ, $\boldsymbol{\sigma}$, f and ε_m^p at a material point and at any instant of time. We obtain a semidiscrete formulation of the problem by using the Galerkin method which results in a set of coupled and nonlinear ordinary differential equations. We employed the lumped mass matrix obtained by using the row sum technique, and evaluated various integrals over an element by using the 3-point quadrature rule. At each node

point in the mesh we have 9 unknowns, namely, ρ, $\mathbf{v}$, θ, $\boldsymbol{\sigma}$, f and ε_m^p. Thus the number of ordinary differential equations equals 9 times the number of nodes. These are integrated with respect to time t by using the subroutine LSODE included in the package ODEPACK. In LSODE, variables ATOL and RTOL that control the absolute and relative errors in the solution vector were each set equal to 10^{-6}. The initial discretization of the domain consisted of uniform 3-noded triangular elements, but subsequent meshes were refined adaptively with the area of the element generated being inversely proportional to the value of $\dot{\varepsilon}_m^p$ at its centroid. Thus the mesh generated had fine elements within the severely deforming region and coarse elements elsewhere. The finite element mesh was refined whenever the porosity at the block centroid increased by a preassigned amount, and the computations were stopped when the porosity at any point in the domain reached the critical value f_f. Depending upon the initial distribution of f, at most six mesh refinements had to be performed. The values of solution variables ρ, $\mathbf{v}$, θ, $\boldsymbol{\sigma}$, f and ε_m^p at the newly created nodes were computed by first ascertaining to which element in the old mesh they belonged, and then by using the interpolation method to find values at the newly generated nodes.

4. Numerical results and discussion

When computing numerical results, we assigned following values to various geometric and material parameters:

$$
\begin{aligned}
\sigma_0 &= 333\,\text{MPa}, \quad E = 210\,\text{GPa}, \quad \nu = 0.27, \quad \nu_s = 6.67\times 10^{-4}/^\circ\text{C},\\
\rho_r &= 7800\,\text{kg/m}^3, \quad k = 49.2\,\text{W/m}^\circ\text{C}, \quad c = 473\,\text{J/kg}^\circ\text{C},\\
b &= 10000\,\text{s}, \quad m = 0.025, \quad n = 0.02, \quad f_2 = 0.04, \quad s_2 = 0.1,\\
e_N &= 0.5, \quad \varepsilon_y = 0.017, \quad \beta_1 = 1.5, \quad \beta_2 = 1.0, \quad f_c = 0.15,\\
f_f &= 0.35, \quad f_u^* = \frac{2}{3}, \quad H = 5\,\text{mm}, \quad t_r = 0.005\,H/v_0.
\end{aligned}
\tag{4.1}
$$

The aforestated values assigned to different material parameters are for a typical steel. The value of ν_s equals the reciprocal of the melting temperature, taken here to be 1500°C, of steel. For $v_0 = 25\,\text{m/s}$, the nominal strain-rate equals $5000\,\text{s}^{-1}$ and the rise time for the axial speed at the top surface to reach its steady value equals one μs.

Figure 2 depicts the effect of initial porosity distribution upon the load-displacement curve for a defect-free homogeneous specimen. The ordinate is the total axial force required to pull the specimen, and the abscissa is the average strain. In this case the deformations of the body stayed homogeneous, thus no mesh refinement was carried out. The plotted results are for a fixed mesh of 1600 uniform constant strain triangular elements. These results evince that higher values of the initial porosity facilitate plastic deformations of the body, thereby

making the system more dissipative, and oscillations in the applied load die out quicker. Subsequent to the initial peak in the load, the average load keeps on decreasing with increasing axial strain because of the softening induced due to the rise in the values of the porosity and the temperature of the body.

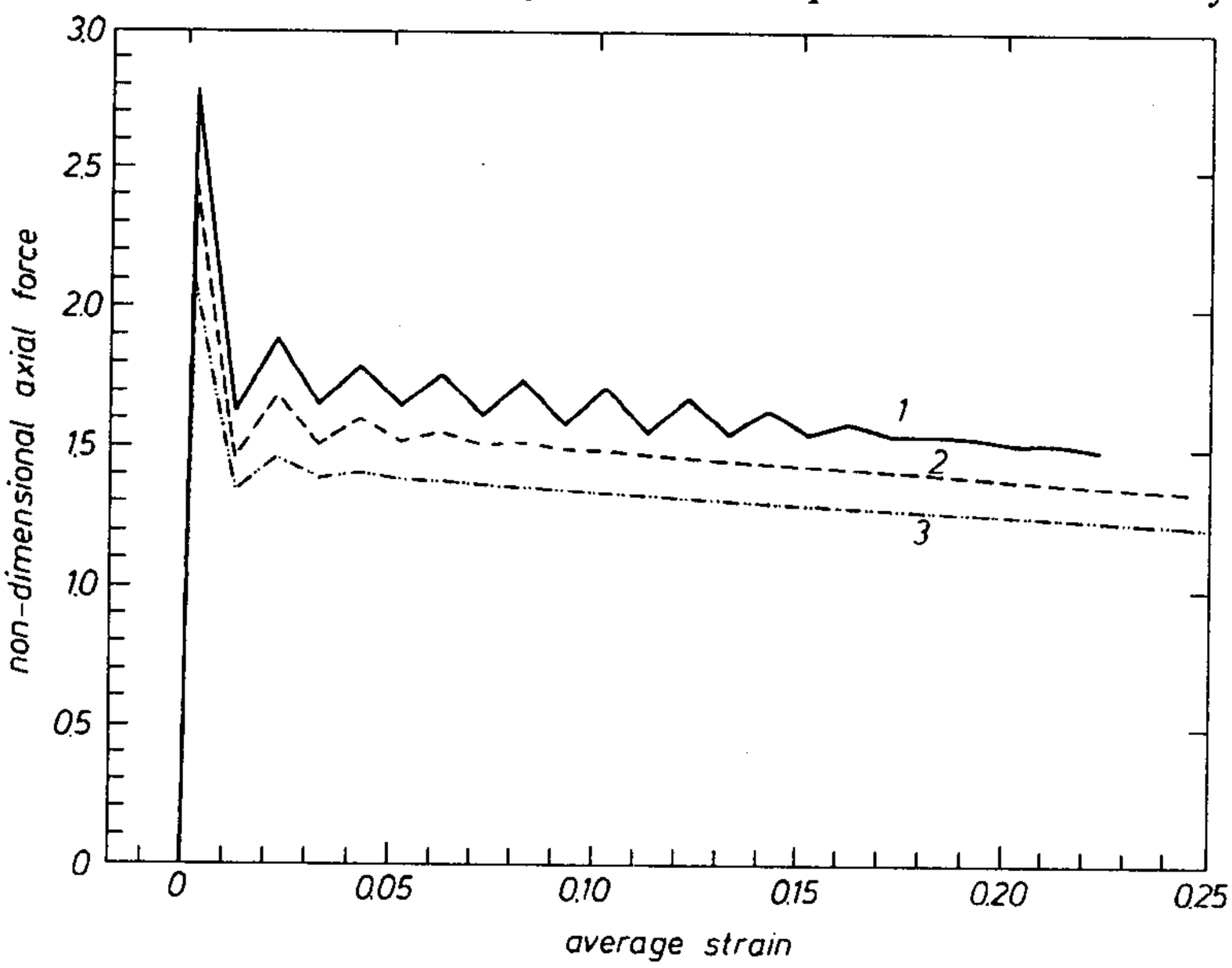

FIG. 2. Axial load vs. time for homogeneous deformations of the body at a nominal strain-rate of $5000\,s^{-1}$ and for three distributions of the initial porosity. *1* – initial porosity = 0.00, *2* – initial porosity = 0.05, *3* – initial porosity = 0.10.

4.1. Effect of nominal strain-rate and initial porosity distribution

In Fig. 3 we have plotted the history of the axial load required to pull the bar at a speed of either 5 m/s or 25 m/s and for three values of the initial porosity. In each case the initial porosity f is nonuniform with the highest value of f occurring at the block centroid, and it quickly decreases to the uniform value at a small distance from the block centroid. We attribute the oscillations of higher amplitude and longer duration at $v_0 = 25$ m/s to the predominance of inertia effects. At the lower value 5 m/s of v_0, after the initial rise in the load because of the increase in the axial speed, the load decreases gradually for each one of the three values of the initial porosity distribution. We note that for a nonporous thermoviscoplastic material BATRA [33] pointed out that inertia forces start playing a noticeable role at a nominal strain-rate of $5000\,s^{-1}$. Just when the axial load began to drop suddenly, the value of f at a node point adjacent to the block centroid reached f_f and the computations were stopped. Because of this we do not see in plots of Fig. 3 the precipitous drop in the load usually associated with the initiation of the localization of the deformation. As will be shown below, the deformation does localize in a narrow band.

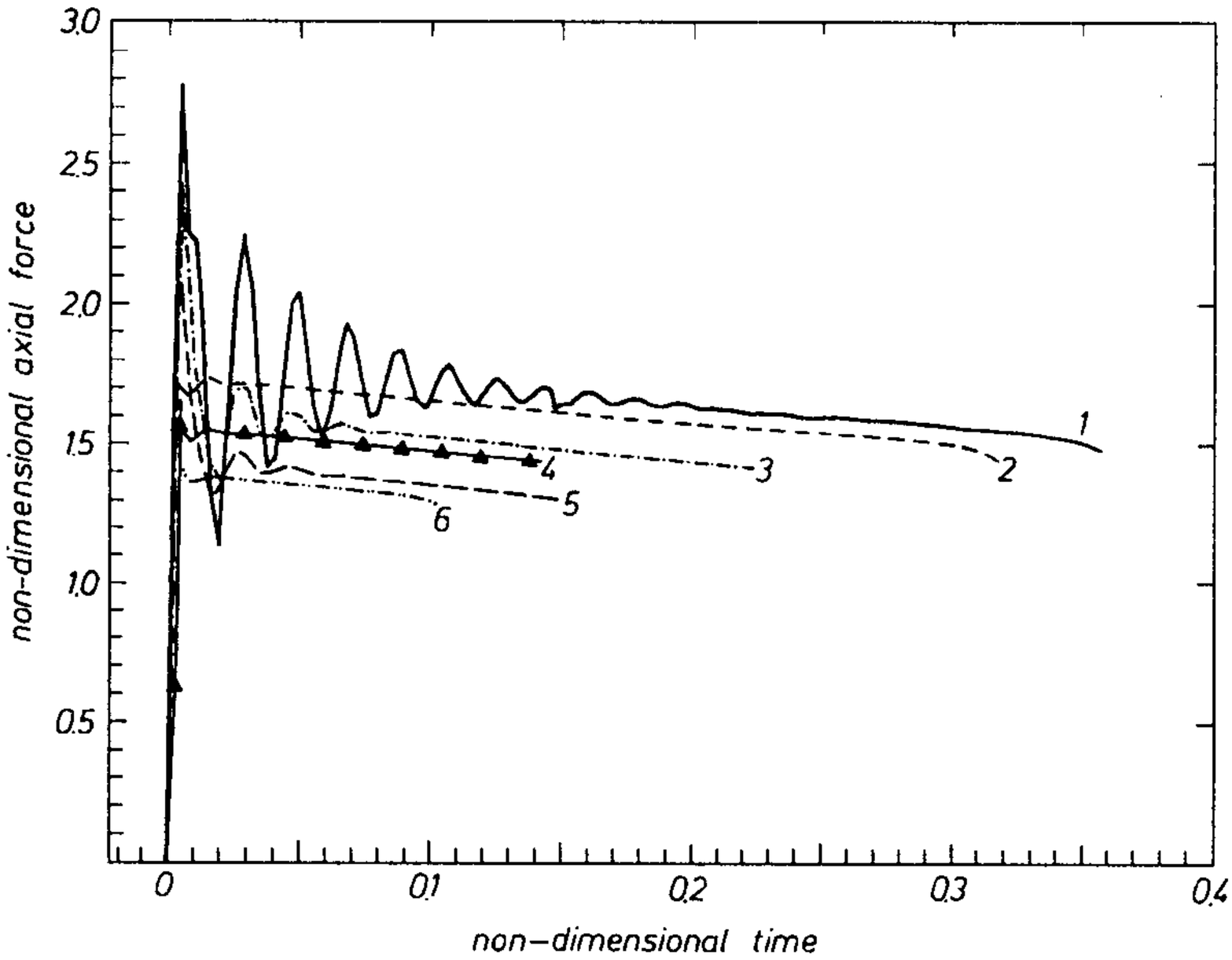

FIG. 3. Axial load vs. time for three distributions of the initial porosity and at nominal strain-rates of $500\,s^{-1}$ and $5000\,s^{-1}$.

1 – $f = 0.025(1 - r^2)^9 \exp(-5r^2)$, $v_0 = 25$ m/s,
2 – $f = 0.025(1 - r^2)^9 \exp(-5r^2)$, $v_0 = 5$ m/s,
3 – $f = 0.05 + 0.025(1 - r^2)^9 \exp(-5r^2)$, $v_0 = 25$ m/s,
4 – $f = 0.05 + 0.025(1 - r^2)^9 \exp(-5r^2)$, $v_0 = 5$ m/s,
5 – $f = 0.1 + 0.025(1 - r^2)^9 \exp(-5r^2)$, $v_0 = 25$ m/s,
6 – $f = 0.1 + 0.025(1 - r^2)^9 \exp(-5r^2)$, $v_0 = 5$ m/s.

Figures 4a, 4b and 4c show, respectively, the evolution of the effective plastic strain, temperature, and porosity at the block centroid for the three different distributions of the initial porosity and two values of the axial speed. Each one of these three variables essentially evolves gradually first, and the rate of increase of these quantities picks up substantially once the deformation has begun to localize. For the same value of $f(\mathbf{x}, 0)$, the increase in the nominal strain-rate from $500\,s^{-1}$ to $5000\,s^{-1}$ delays the initiation of the localization of the deformation, primarily due to the effect of inertia forces. For a given strain-rate of $500\,s^{-1}$ or $5000\,s^{-1}$, an increase in the value of $f(\mathbf{x}.0)$ causes the localization of the deformation to occur earlier. This is because a more porous material undergoes plastic deformation at a lower value of σ_m, thus facilitating the growth and nucleation of voids and also causing the material to heat up sooner, both of which enhance further its plastic deformations. Hence it is a self-feeding mechanism.

In order to illustrate that the deformation does localize and to depict how the finite element meshes adapt to the deformations, we show below results for the case of

$$f(\mathbf{x}, 0) = 0.025(1 - r^2)^9 \exp(-5r^2), \qquad v_0 = 25\,\text{m/s}. \tag{4.2}$$

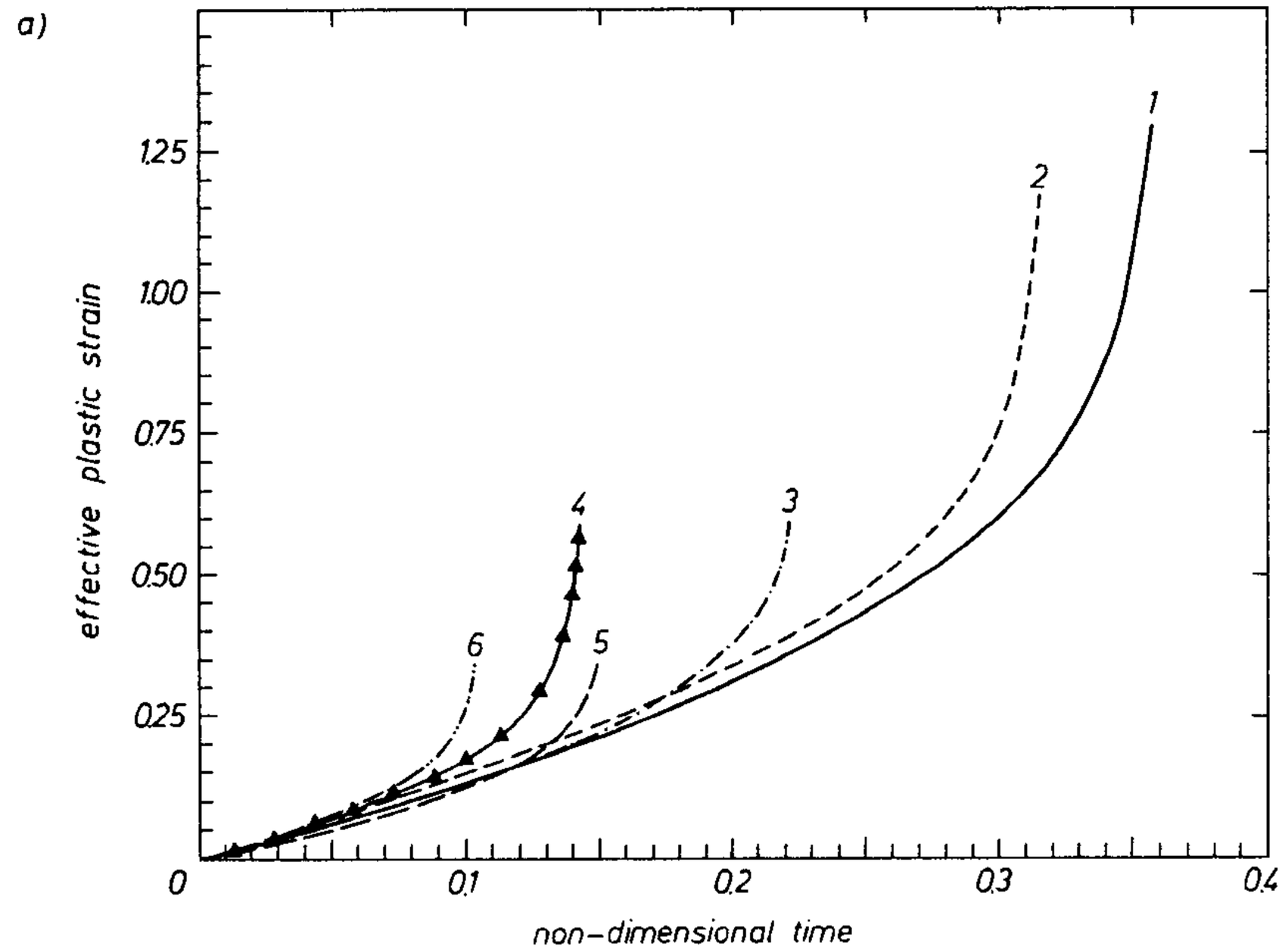

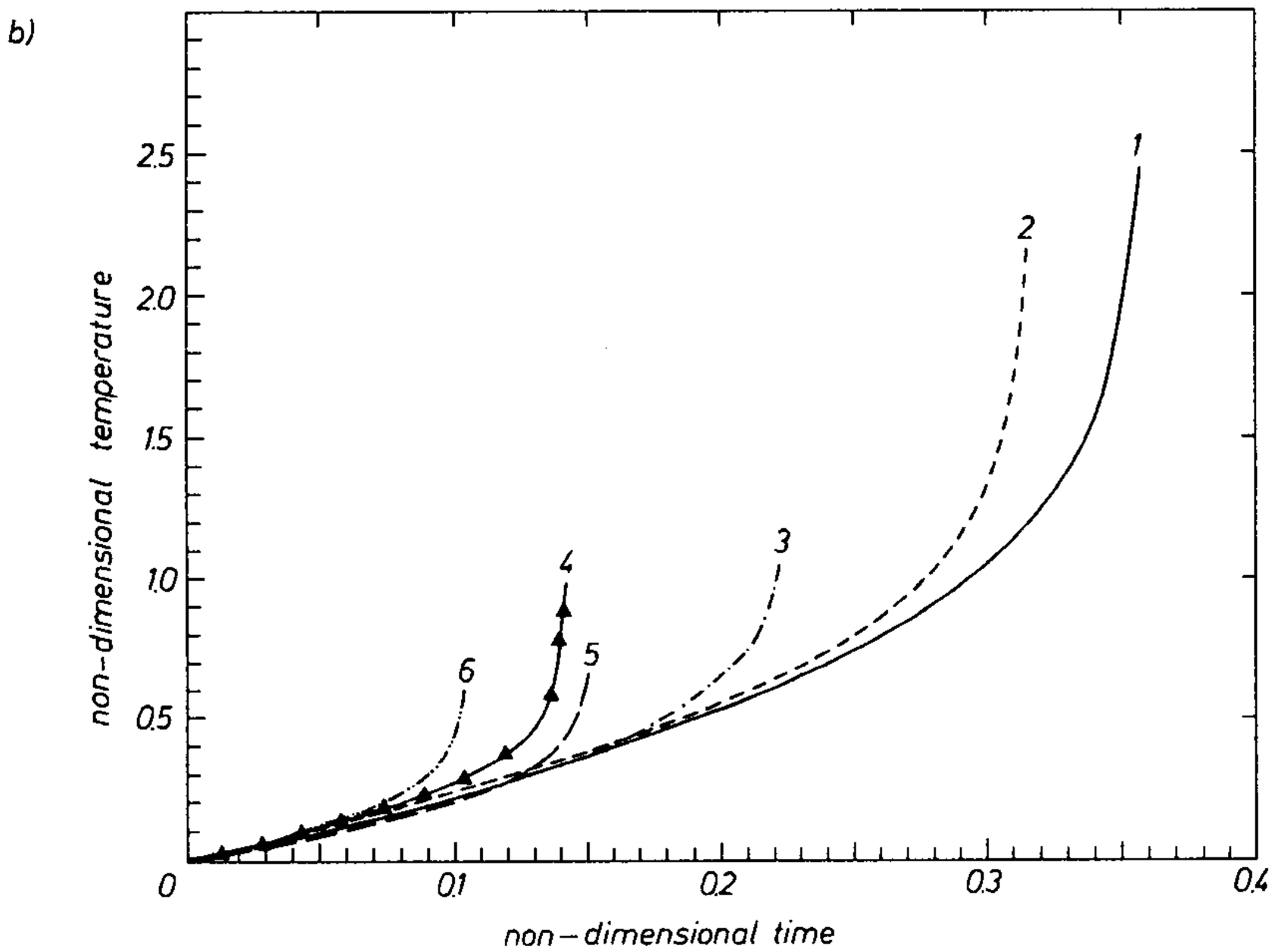

FIG. 4. Evolution at the block centroid of (a) the effective plastic strain, (b) the temperature for three distributions of the initial porosity and at nominal strain-rates of $500\,s^{-1}$ and $5000\,s^{-1}$.

1 – $f = 0.025(1 - r^2)^9 \exp(-5r^2)$, $v_0 = 25$ m/s,
2 – $f = 0.025(1 - r^2)^9 \exp(-5r^2)$, $v_0 = 5$ m/s,
3 – $f = 0.05 + 0.025(1 - r^2)^9 \exp(-5r^2)$, $v_0 = 25$ m/s,
4 – $f = 0.05 + 0.025(1 - r^2)^9 \exp(-5r^2)$, $v_0 = 5$ m/s,
5 – $f = 0.1 + 0.025(1 - r^2)^9 \exp(-5r^2)$, $v_0 = 25$ m/s,
6 – $f = 0.1 + 0.025(1 - r^2)^9 \exp(-5r^2)$, $v_0 = 5$ m/s.

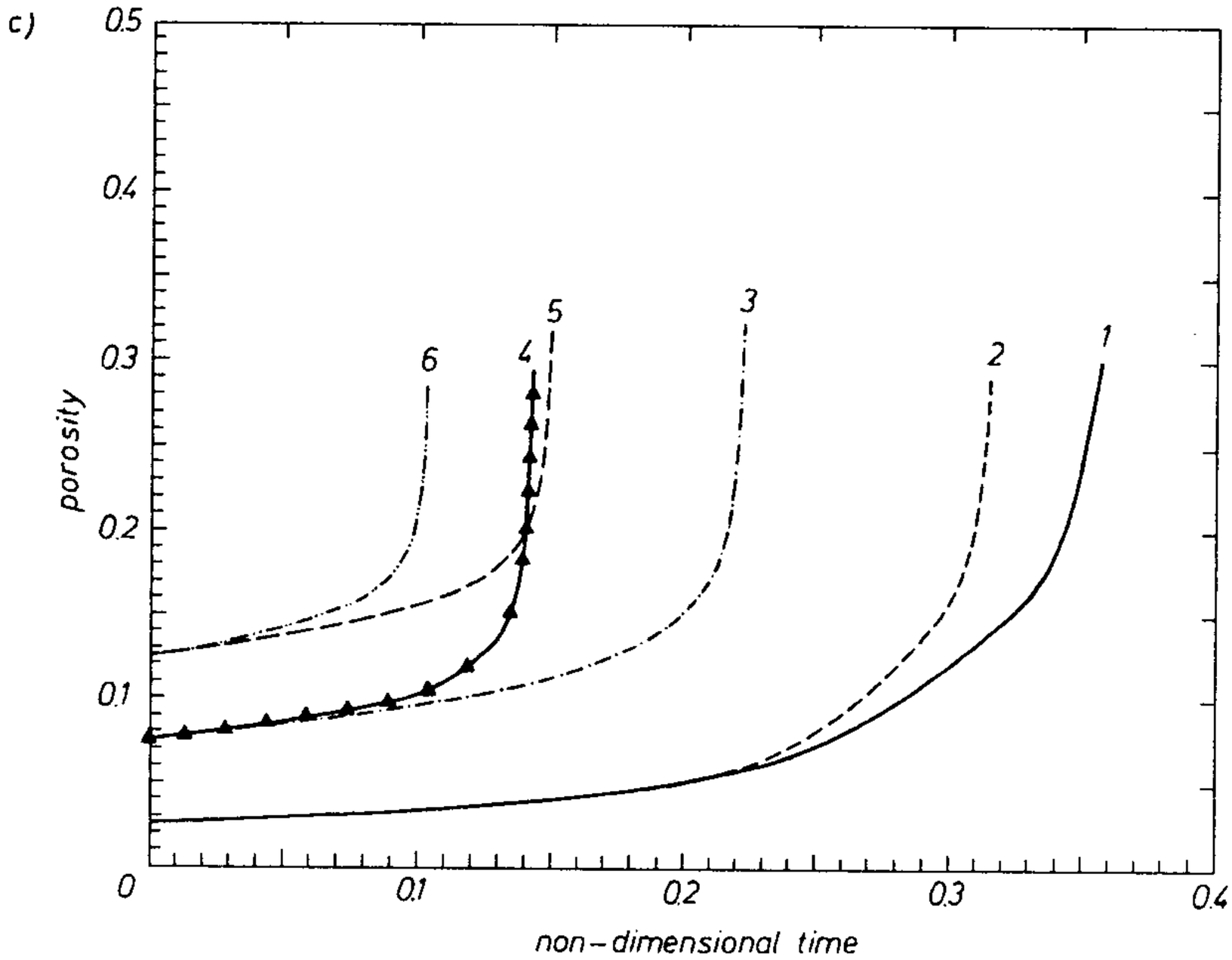

FIG. 4 [cont.]. Evolution at the block centroid of (c) the porosity for three distributions of the initial porosity and at nominal strain-rates of $500\,s^{-1}$ and $5000\,s^{-1}$.

$1 - \quad f = 0.025(1 - r^2)^9 \exp(-5r^2), \qquad v_0 = 25\,\text{m/s},$
$2 - \quad f = 0.025(1 - r^2)^9 \exp(-5r^2), \qquad v_0 = 5\,\text{m/s},$
$3 - \quad f = 0.05 + 0.025(1 - r^2)^9 \exp(-5r^2), \qquad v_0 = 25\,\text{m/s},$
$4 - \quad f = 0.05 + 0.025(1 - r^2)^9 \exp(-5r^2), \qquad v_0 = 5\,\text{m/s},$
$5 - \quad f = 0.1 + 0.025(1 - r^2)^9 \exp(-5r^2), \qquad v_0 = 25\,\text{m/s},$
$6 - \quad f = 0.1 + 0.025(1 - r^2)^9 \exp(-5r^2), \qquad v_0 = 5\,\text{m/s}.$

Figures 5a, 5b, 5c and 5d show the finite element meshes generated at non-dimensional times $t = 0.198$, 0.285, 0.339 and 0.357. We note that the initial mesh consisted of 1600 uniform triangular elements. The finite element mesh was refined whenever the porosity f at the block centroid had increased by 0.025, a criterion chosen somewhat arbitrarily. The mesh was refined by using the code developed by BATRA and KO [34] which generates meshes such that the area of an element is inversely proportional to the value of a deformation-rate measure, here taken to be $\dot{\varepsilon}_m$, at the element centroid. It is clear then that a narrow region of the material is deforming severely at times $t = 0.339$ and 0.357. As stated earlier, computations were stopped when the porosity at any point in the deforming region reached the critical value f_f. This implies failure of the material at a point which does not necessarily result in the instantaneous failure of the block. Figures 6a, 6b, 6c and 6d evince the distribution of the velocity within the deforming region at the aforestated four values of the non-dimensional time t. Initially, because of the lateral motion of the block, the velocity component in the horizontal direction has a significant value everywhere. However, once the deformation has started to localize, the body is essentially divided into three

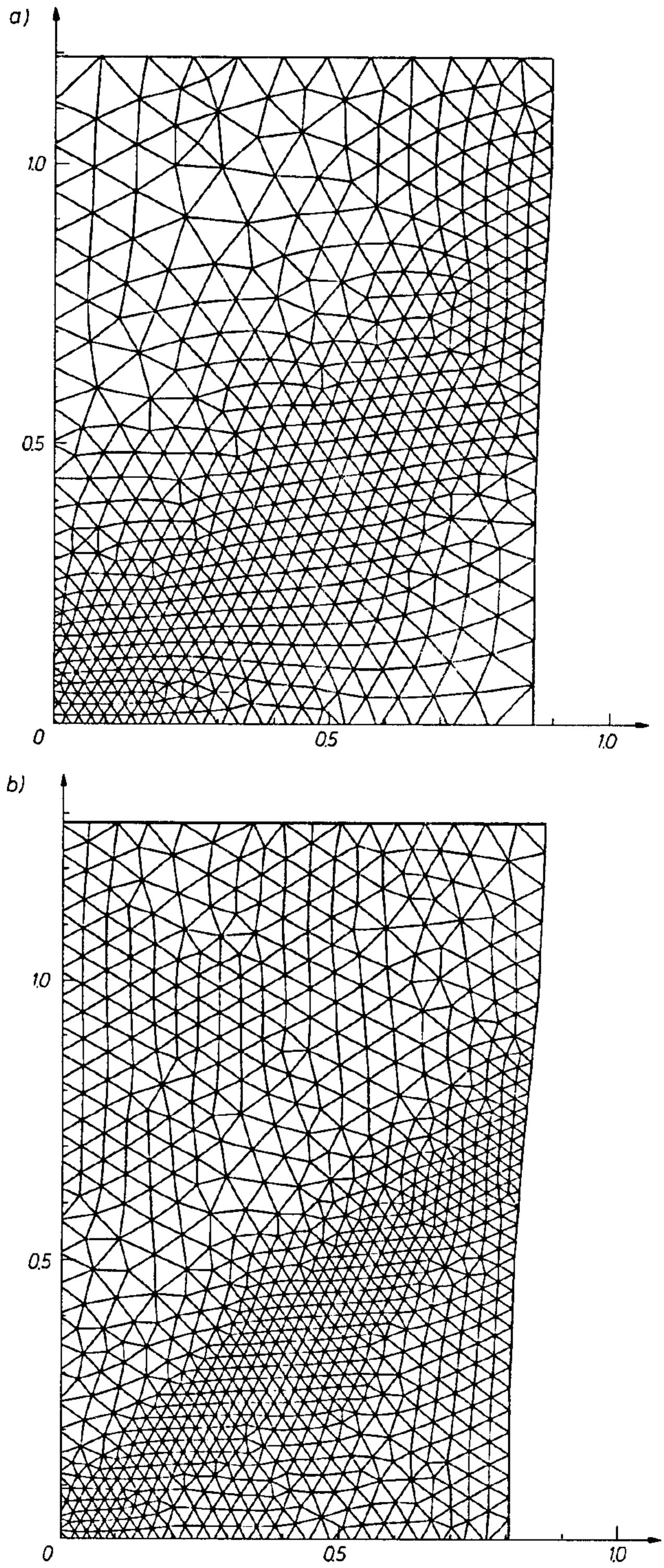

FIG. 5. Adaptively refined meshes at non-dimensional times (a) $t = 0.198$, (b) $t = 0.285$.

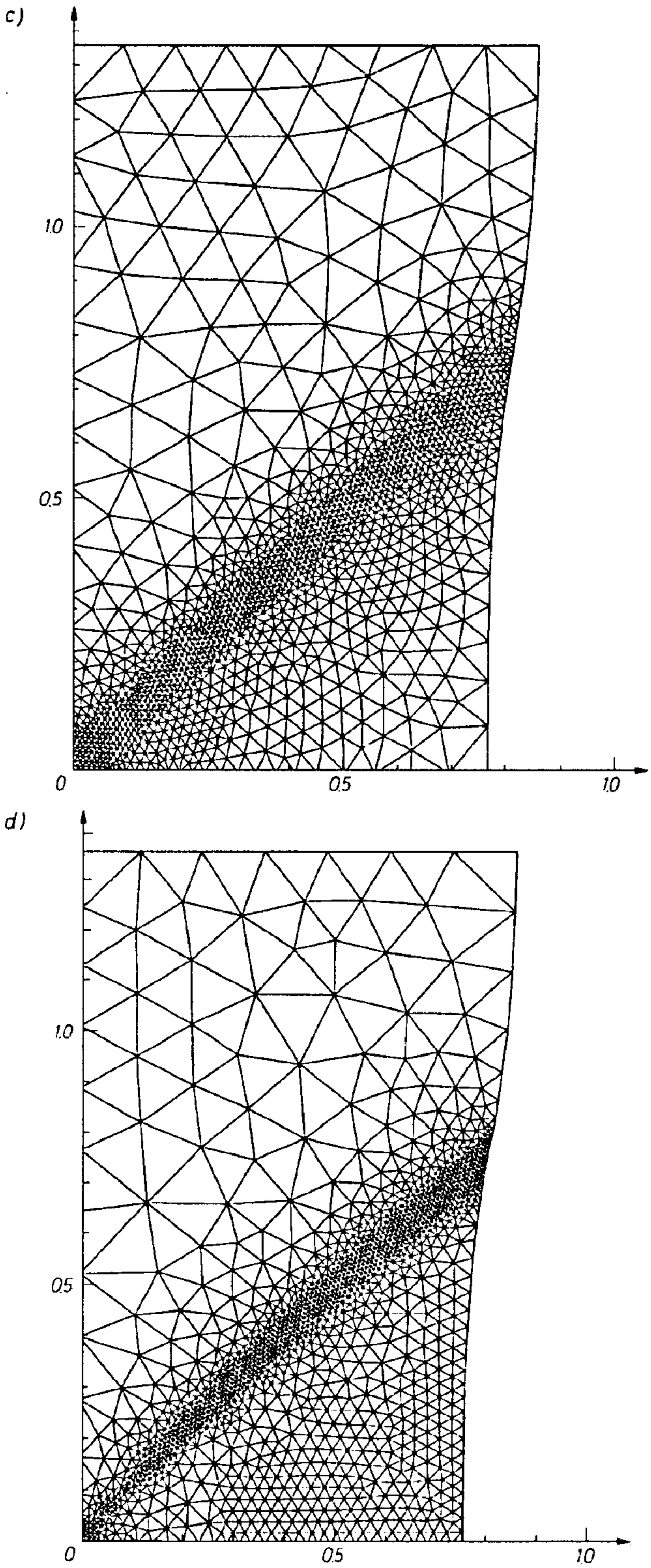

FIG. 5 [cont.]. Adaptively refined meshes at non-dimensional times (c) $t = 0.339$ and (d) $t = 0.357$.

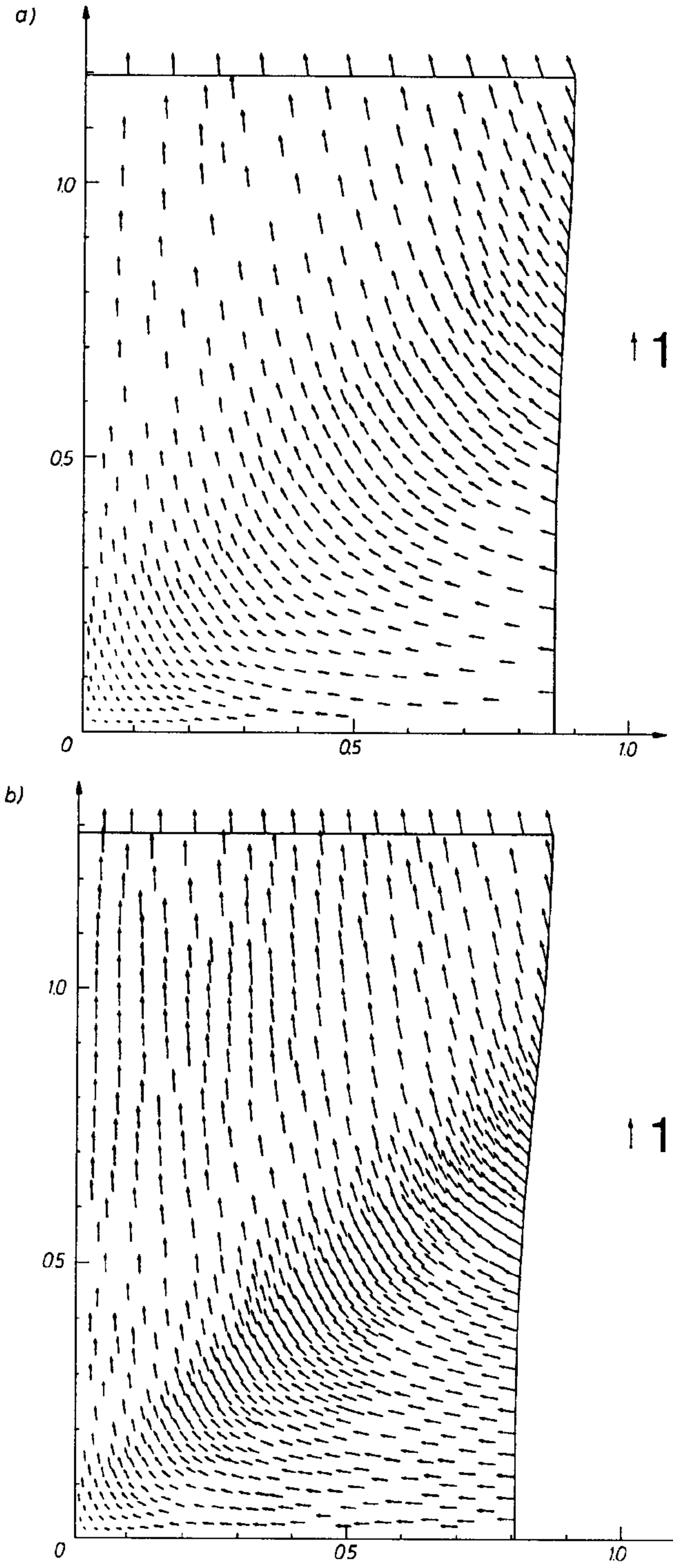

FIG. 6. Velocity distribution in the deforming region at non-dimensional times (a) $t = 0.198$, (b) $t = 0.285$.

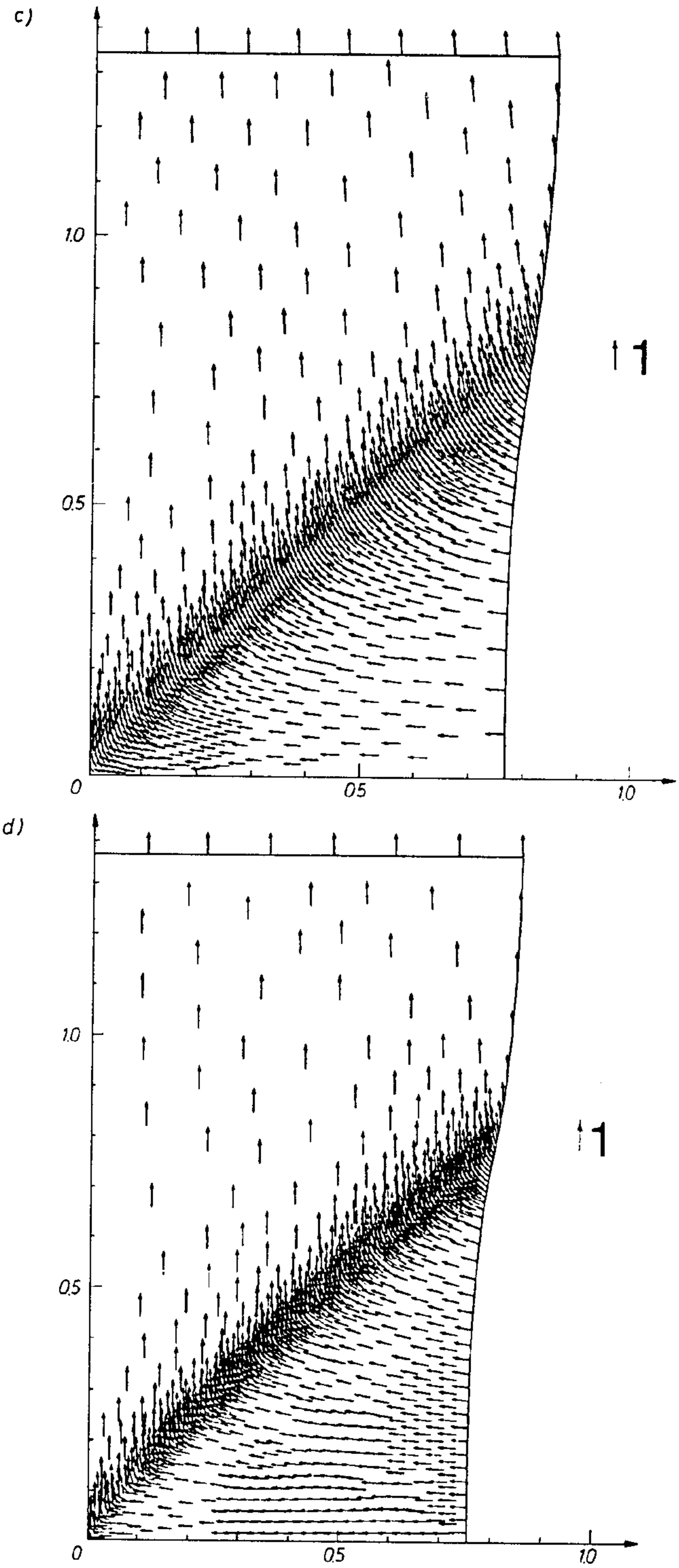

FIG. 6 [cont.] Velocity distribution in the deforming region at non-dimensional times (c) $t = 0.339$ and (d) $t = 0.357$.

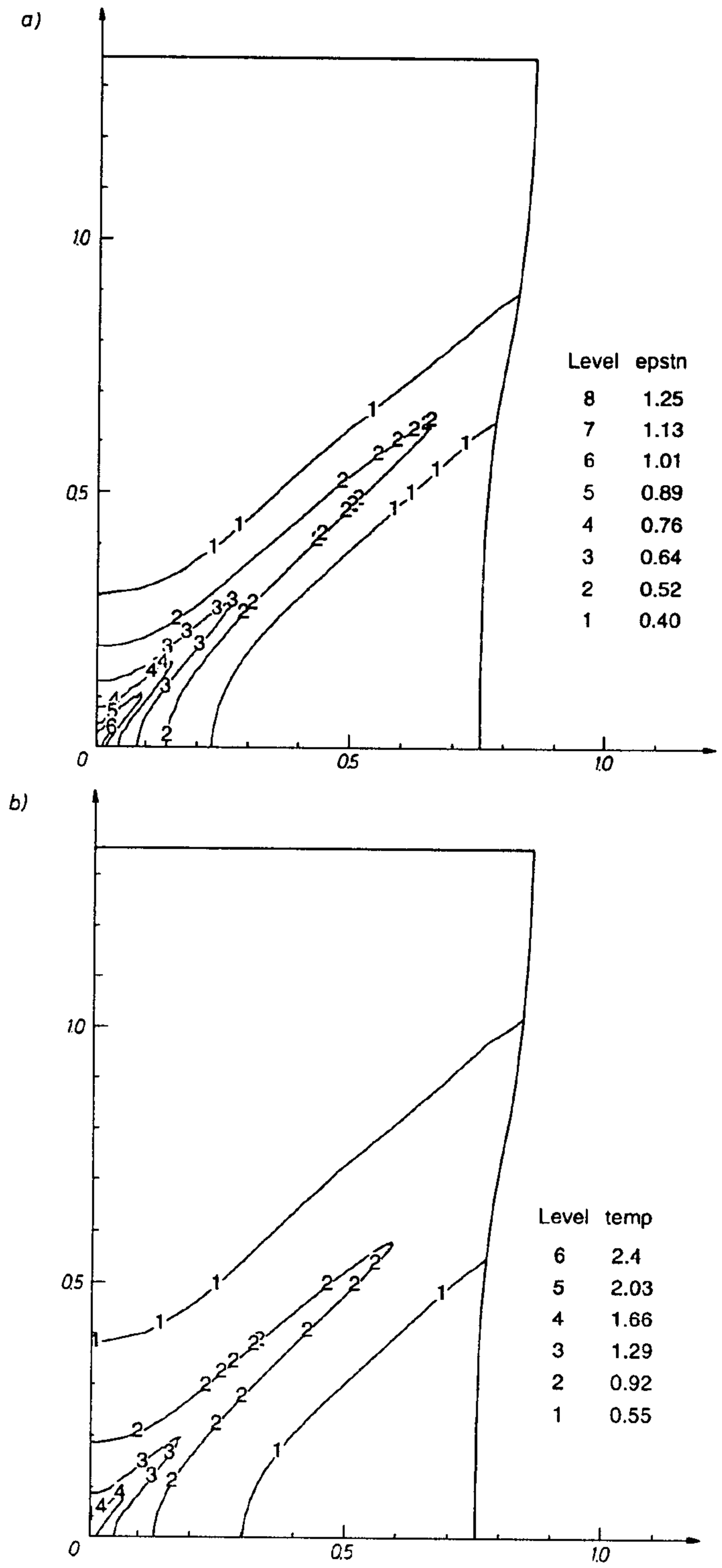

FIG. 7. Contours of (a) the effective plastic strain and (b) the temperature.

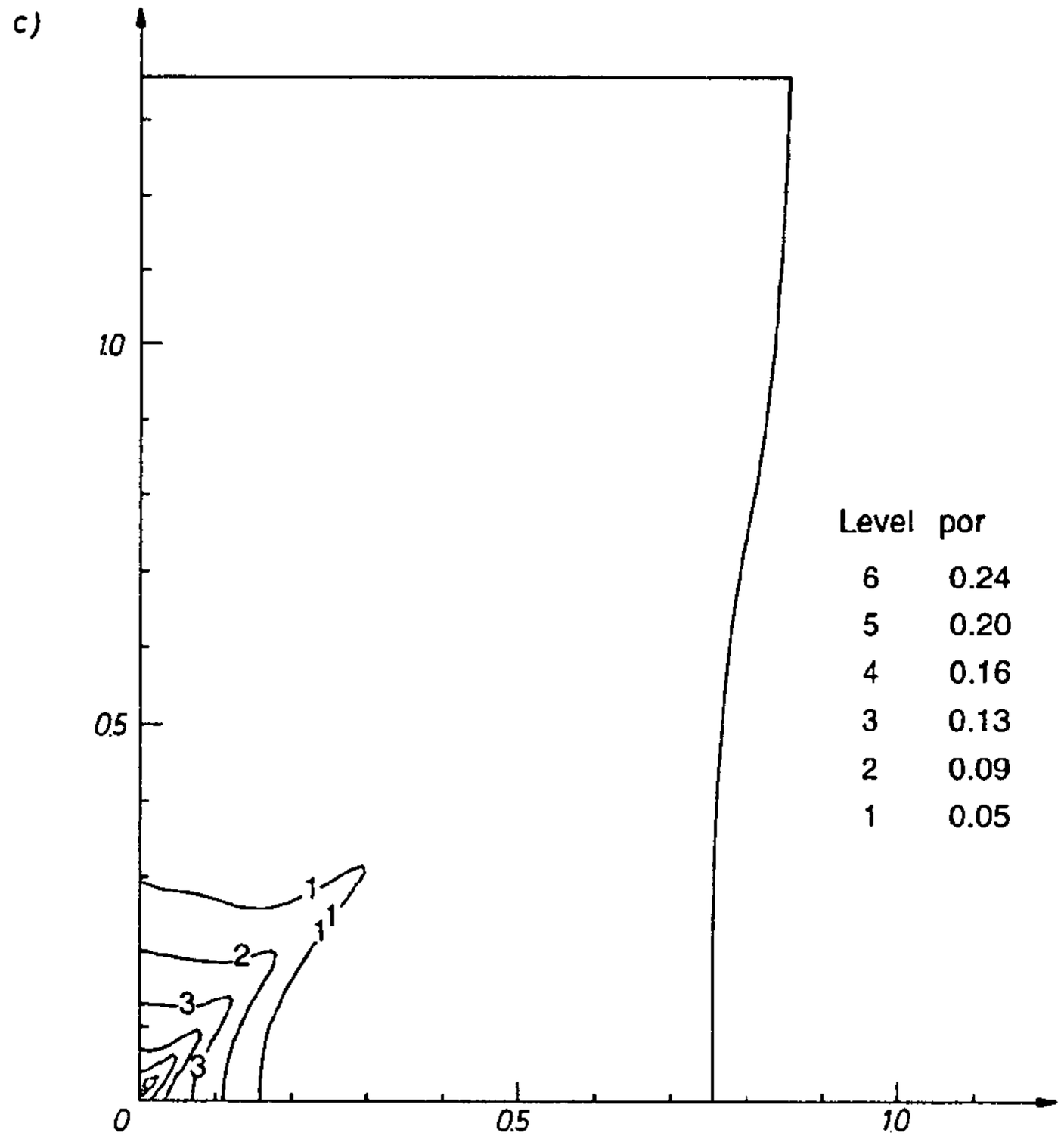

FIG. 7 [cont.]. Contours of (c) the porosity at non-dimensional time $t = 0.357$.

regions. In the region above the shear band, the material particles are moving nearly vertically, and those below the band – horizontally. Within the band, the velocity changes direction sharply.

Contours of the effective plastic strain (epstn), temperature rise, and the porosity within the deforming region at time $t = 0.357$ are shown in Figs. 7a, 7b, and 7c. It is clear that the strain near the block centroid is quite high. However, the temperature rise there is only $2.4 \times 89.8 = 216°C$, and the porosity has increased significantly only in a very narrow region surrounding the block center.

4.2. Effect of strain-induced void nucleation

In order to present the effect of the softening caused by the plastic strain-controlled nucleation of voids, we have plotted in Fig. 8 the evolution of the applied axial force at the top surface and that of temperature, effective plastic strain and porosity at the block centroid for the two cases: (i) $f_2 = 0$, and (ii) $f_2 = 0.04$. It is apparent that the consideration of strain-induced void nucleation enhances the onset of the localization of the deformation, as shown by the sharp rise in the rate of increase of the temperature, effective plastic strain and the porosity at the block centroid.

a)

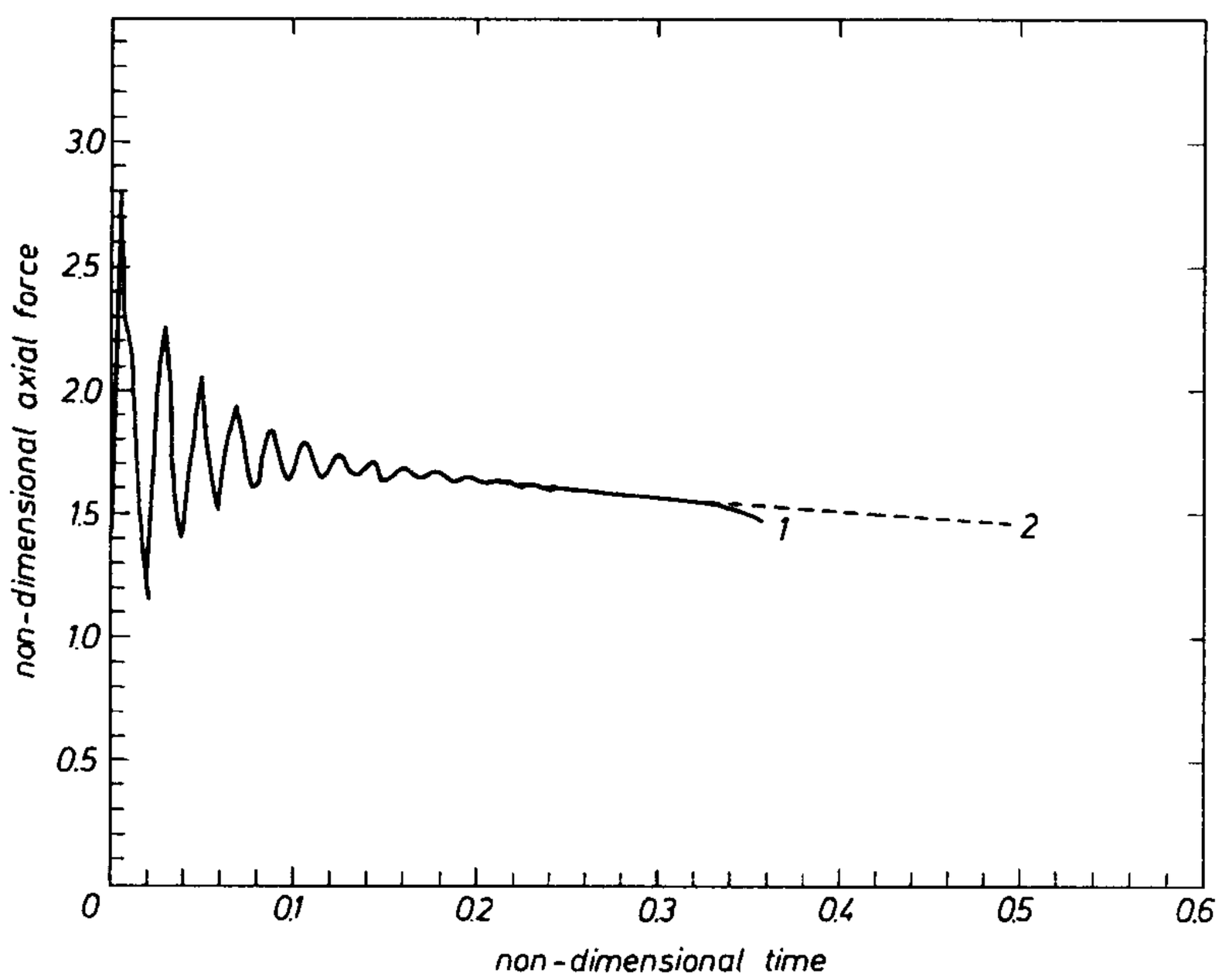

b)

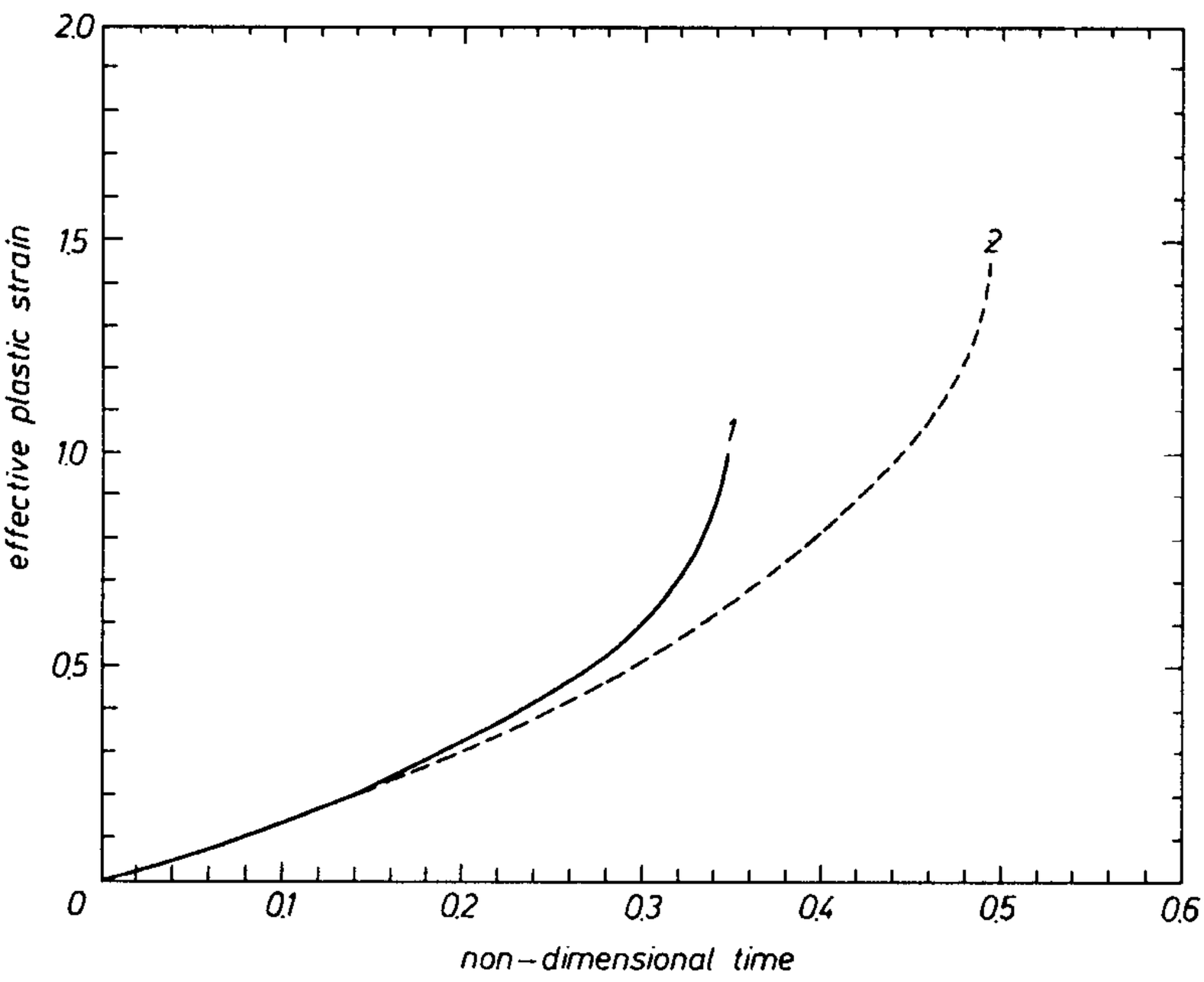

[FIG. 8a,b]

1 – with strain-induced void nucleation, *2* – without strain-induced void nucleation.

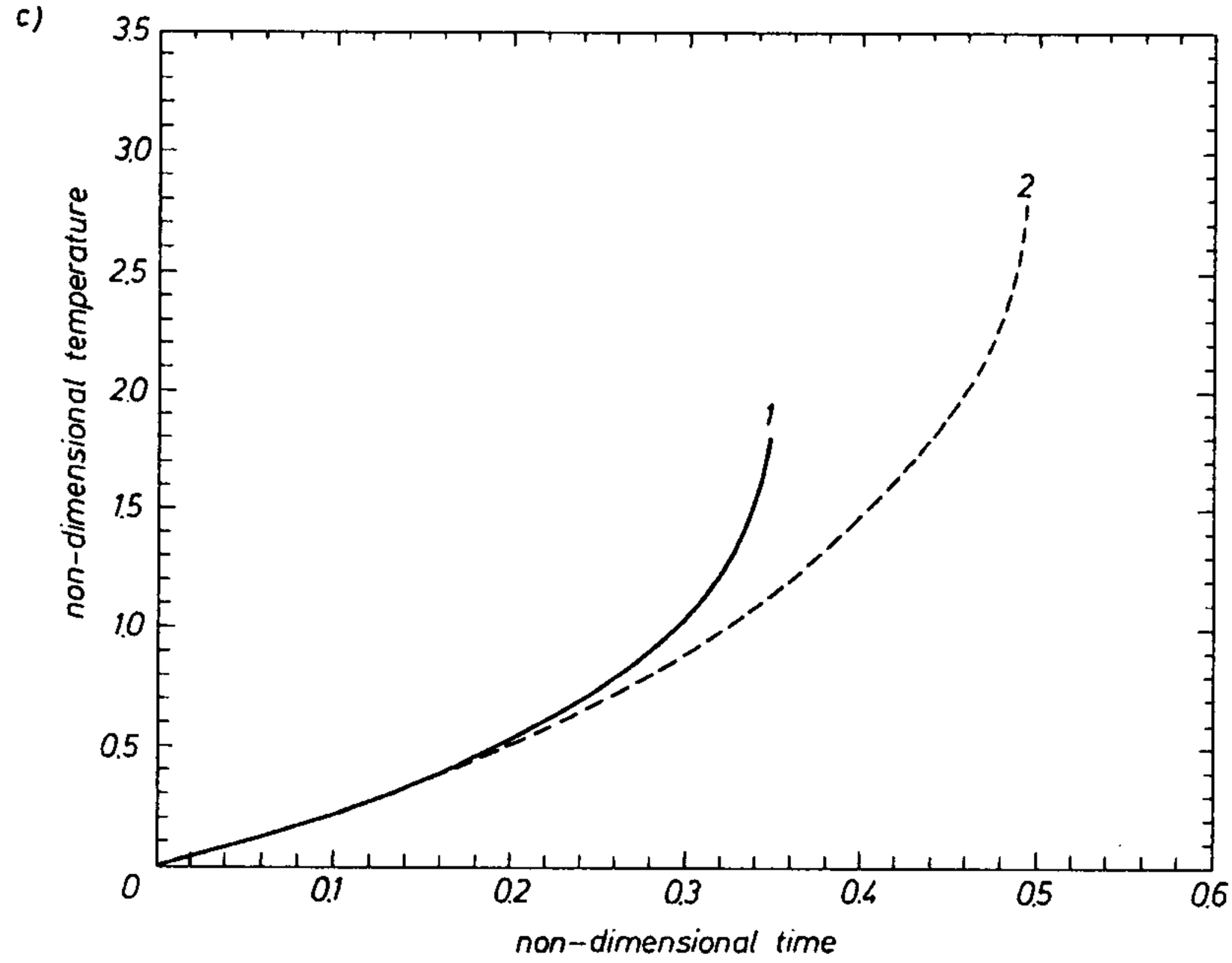

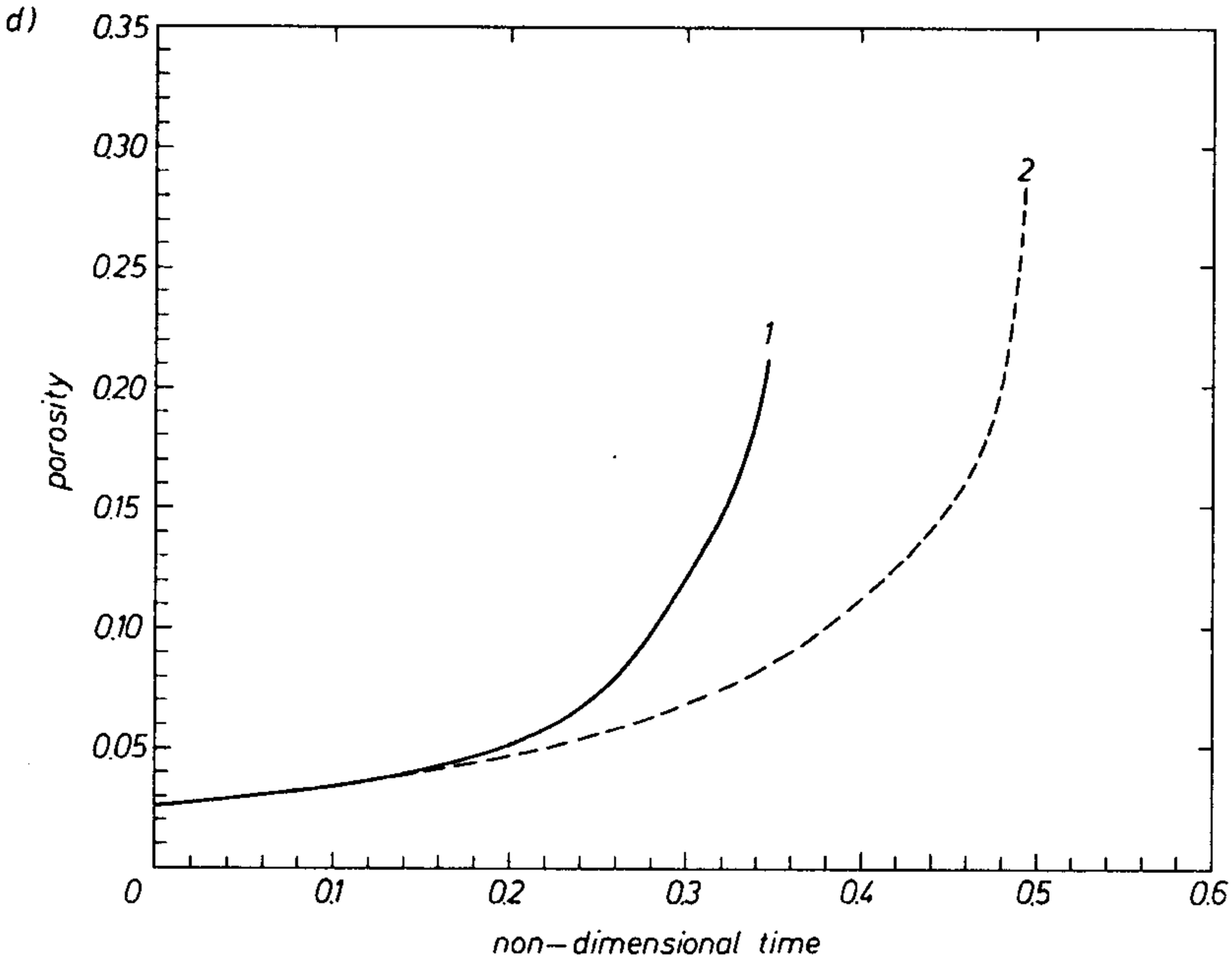

FIG. 8. (a) Variation of the non-dimensional applied axial force with non-dimensional time, both with and without strain-induced void nucleation; (b,c,d) evolution at the block centroid of the effective plastic strain, the temperature, and the porosity with and without strain-induced void nucleation. *1* – with strain-induced void nucleation, *2* – without strain-induced void nucleation.

4.3. Thermal softening vs. softening due to porosity change

For the choice (4.1) of parameters we assessed the effect of softening caused by the rise in temperature versus that induced due to the increase in porosity by performing two sets of calculations, one with $\nu_s = 0$ and the other with $f(\mathbf{x}, t) \equiv 0$. The material defect for these computations was modelled by assuming that the yield stress $\hat{\sigma}_0$ in a quasistatic simple compression test of material particles in a small region around the block centroid was given by

$$\begin{aligned} \hat{\sigma}_0(\mathbf{X}) &= \sigma_0 \left(1 - 0.1(1 - r^2)^9 e^{-5r^2}\right), \qquad r^2 \equiv (X_1^2 + X_2^2)/H^2 \leq 1, \\ &= \sigma_0, \qquad r \geq 1. \end{aligned}$$

In Fig. 9, we have plotted the evolution of the applied axial force, and that of the effective plastic strain and the temperature rise at the block centroid for the two cases with $v_0 = 25$ m/s. It is clear that for the parameters considered herein, the softening due to the increase in porosity is considerably higher than that caused by the rise in the temperature. Whereas a shear band initiates, as indicated by the rise in the rate of increase of the effective plastic strain and of the temperature at the block centroid at non-dimensional time $t \simeq 0.5$ when softening is caused by the change in porosity, no shear band forms till a non-dimensional time of 0.5 when the softening is induced by the temperature rise, since both the effective plastic strain and the temperature at the block centroid increase

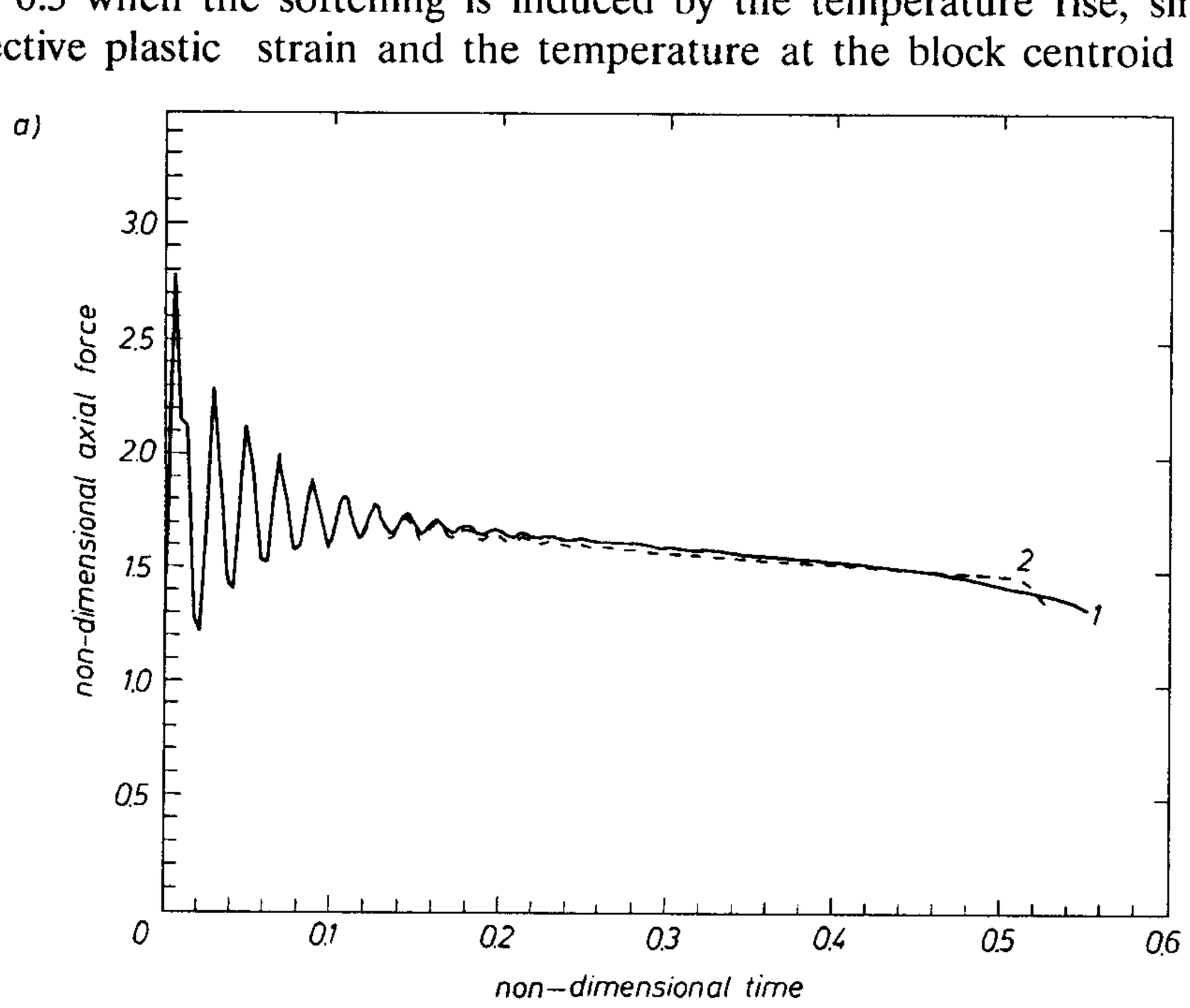

[FIG. 9a]

1 – no thermal softening, *2* – thermal softening only.

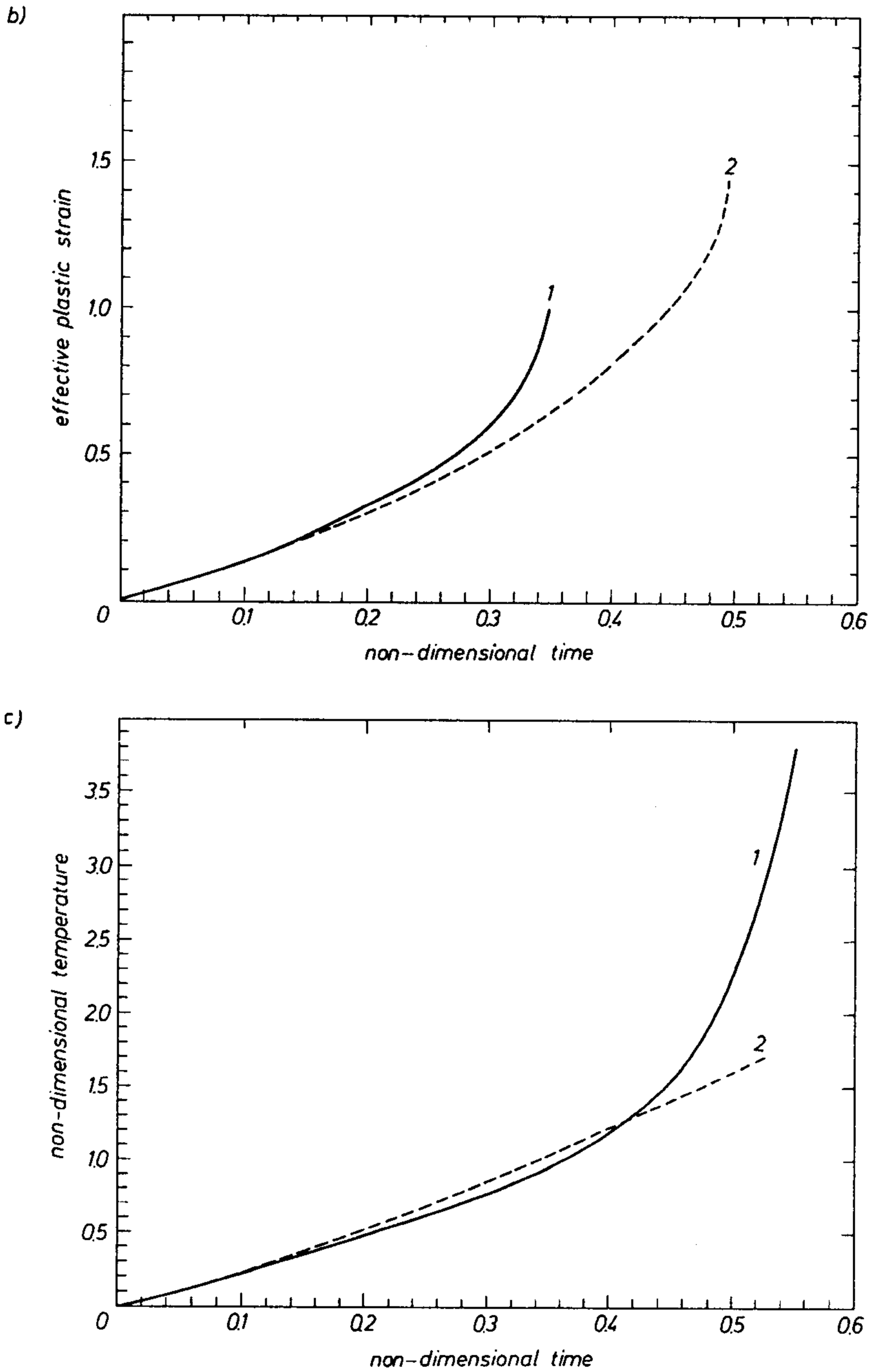

FIG. 9. Variation of (a) the non-dimensional applied axial force vs. non-dimensional time, (b) the effective plastic strain at the block centroid vs. time, *1* – with strain-induced void nucleation, *2* – without strain-induced void nucleation and (c) the temperature at the block centroid vs. time, both with and without thermal softening effects considered, *1* – no thermal softening, *2* – thermal softening only.

essentially linearly with time. It is possible that a band will initiate at a later time. Thus for the values of material parameters chosen for this study, softening caused by the growth and nucleation of voids is stronger than that induced by the temperature rise.

5. Conclusions

We have studied dynamic finite plane strain thermomechanical deformations of a porous viscoplastic body deformed in tension. The material is modelled by the Gurson-Tvergaard-Needleman yield function with the flow stress for the matrix material given by a relation similar to that proposed by BATRA [28]. When the dependence of material parameters upon the porosity is considered, they are assumed to be independent of temperature. The problem formulation includes the effect of inertia forces and heat conduction.

The coupled nonlinear partial differential equations governing the deformations of the body are reduced to a set of coupled nonlinear ordinary differential equations by using the Galerkin method. These are integrated with respect to time t by using the IMSL subroutine LSODE. The finite element mesh has been refined adaptively.

It is found that inertia forces play a dominant role at a nominal strain-rate $\dot{\gamma}_{avg}$ of $5000\,s^{-1}$, but a negligible role when $\dot{\gamma}_{avg} = 1000\,s^{-1}$. An increase in the initial value of the porosity makes the system more dissipative in the sense that oscillations in the applied axial force die out quickly. The shear band forms at a lower value of the nominal strain when the initial porosity is increased. Once a shear band has developed, the material above the shear band moves upwards with the velocity imposed on the top surface, and that below the band moves horizontally to the left, with the velocity changing sharply from essentially horizontal to nearly vertical on the two sides of the severely deforming region. The computations were stopped when the porosity at a point reached a critical value. The material at the center necked. The softening caused by the increase in the porosity is more than that induced by the rise in the temperature of the body, at least, for the values assigned to material parameters herein.

Acknowledgement

This work was supported by the U.S. Army Research Office grant DAAL03-91-G-0084 and the National Science Foundation grant MSS9121279 to the University of Missouri-Rolla.

References

1. R.E. WINTER, Philos. Mag., **31**, 765, 1975.
2. S.P. TIMOTHY and I.M. HUTCHINGS, Acta Metall., **33**, 667, 1985.
3. H.A. GREBE, H. PAK and M.A. MEYERS, Metal. Trans., **16A**, 761, 1985.
4. L. SEAMAN, D.R. CURRAN and D.A. SHOCKEY, J. Appl. Phys., **47**, 4814, 1976.
5. A. MARCHAND, K. CHO and J. DUFFY, *The formation of adiabatic shear bands in an AISI 1018 cold-rolled steel*, Brown Univ. Report, 1988.
6. K. CHO, Y.C. CHI and J. DUFFY, *Microscopic observations of adiabatic shear bands in three different steels*, Brown Univ. Report, 1988.
7. C.F. TIPPER, *The fracture of metals*, Metallurgica, **39**, 133–138, 1949.
8. K.E. PUTTICK, *Ductile fracture in metals*, Philos. Mag., **4**, 964–969, 1959.
9. K.E. PUTTICK, *The shear component of ductile fracture*, Philos. Mag., **5**, 759–762, 1960.
10. H.C. ROGERS, *Tensile fracture of ductile metals*, Trans. TMS-AIME, **28**, 498–506, 1960.
11. C. ZENER and J.H. HOLLOMON, J. Appl. Phys., **14**, 22, 1944.
12. T.G. SHAWKI and R.J. CLIFTON, Mech. Materials, **8**, 13, 1989.
13. R.C. BATRA and Z.G. ZHU, Int. J. Solids Structures, **27**, 1829, 1991.
14. J.W. NUNZIATO and S.C. COWIN, *A nonlinear theory of elastic materials with voids*, Arch. Rational Mech. Anal., **72**, 175–201, 1979.
15. H.A. KUHN and C.L. DOWNEY, *Deformation characteristics and plasticity theory of sintered powder materials*, Int. J. Powder Metall., **7**, 15–25, 1971.
16. R.J. GREEN, *A plasticity theory for porous solids*, Int. J. Mech. Sci., **14**, 215–224, 1972.
17. A.L. GURSON, *Continuum theory of ductile rupture by void nucleation and growth. Part 1. Yield criteria and flow rules for porous ductile media*, J. Eng. Mater. Technol., **99**, 2–15, 1977.
18. S. SHIMA and M. OYANE, *Plasticity theory for ductile metals*, Int. J. Mech. Sci., **18**, 285–291, 1976.
19. V. TVERGAARD, *Influence of voids on shear band instabilities under plane strain conditions*, Int. J. Fracture, **17**, 389–407, 1981.
20. V. TVERGAARD, *On localization in ductile materials containing spherical voids*, Int. J. Fracture, **18**, 237–252, 1982.
21. V. TVERGAARD and A. NEEDLEMAN, *Analysis of the cup-cone fracture in a round tensile bar*, Acta Metall., **32**, 157–196, 1984.
22. J. PAN, M. SAJE and A. NEEDLEMAN, *Localization of deformation in rate-sensitive porous plastic solids*, Int. J. Fract., **21**, 261–278, 1983.
23. M. SAJE, J. PAN and A. NEEDLEMAN, *Void nucleation effects on shear localization in porous plastic solids*, Int. J. Fracture, **19**, 163–182, 1982.
24. H. KOBAYASHI and B. DODD, *A numerical analysis for the formation of adiabatic shear bands including void nucleation and growth*, Int. J. Impact Engng., **8**, 1–13, 1989.
25. A. ZAVALIANGOS and L. ANAND, *Thermal aspects of shear localization in microporous viscoplastic solids*, Int. J. Num. Meth. Engng., **33**, 595–634, 1992.
26. S.L. PASSMAN and R.C. BATRA, *A thermomechanical theory for a porous anisotropic elastic solid with inclusions*, Arch. Rat. Mech. Anal., **87**, 11–33, 1984.
27. B. BUDIANSKY, *Thermal and thermoelastic properties of isotropic composites*, J. Compos. Mater., **4**, 701–744, 1990.
28. R.C. BATRA, *Steady state penetration of thermoviscoplastic targets*, Computat. Mech., an Int. J., 3, 1–11, 1988.
29. J. LITOŃSKI, Bull. Acad. Polon. Sci., **25**, 7, 1977.
30. C.C. CHU and A. NEEDLEMAN, J. Engng. Mat. and Technol., **102**, 249–256, 1980.
31. G.H. LEROY, *Large scale plastic deformation and fracture for multiaxial stress states*, Ph. D. Thesis, McMaster University, 1978.
32. J.R. FISCHER, *Void nucleation in spheroidized steels during tensile deformation*, Ph. D. Thesis, Brown University, 1980.

33. R.C. BATRA, *Effect of nominal strain-rate on the initiation and growth of adiabatic shear bands in steels*, J. Appl. Mech., **55**, 229–230, 1988.
34. R.C. BATRA and K.I. KO, *An adaptive mesh refinement technique for the analysis of shear bands in plane strain compression of a thermoviscoplastic solid*, Computat. Mech., **10**, 369–379, 1992.

DEPARTMENT OF ENGINEERING SCIENCE AND MECHANICS
VIRGINIA POLYTECHNIC INSTITUTE AND STATE UNIVERSITY, BLACKSBURG, USA.

Received November 17, 1993.